JOURNAL OF GEOPHYSICAL RESEARCH, VOL. 112, A10226, doi:10.1029/2006JA012183, 2007

Reconstruction of the reconnection rate from Cluster measurements: Method improvements

V. V. Ivanova,[1,2] V. S. Semenov,[1] T. Penz,[2,3,4] I. B. Ivanov,[5,6] V. A. Sergeev,[1] M. F. Heyn,[6] C. J. Farrugia,[7] H. K. Biernat,[2,3] R. Nakamura,[2] and W. Baumjohann[2]

Received 6 December 2006; revised 6 June 2007; accepted 13 July 2007; published 31 October 2007.

[1] A remote-sensing method for reconstructing the reconnection rate and the location of X-line from single-spacecraft observations developed recently is extended to a compressible plasma and an asymmetric magnetic field configuration. The method is based on the two-dimensional analytical model of time-dependent Petschek-type magnetic reconnection. The reconstruction technique is applied to a nightside flux transfer event recorded by Cluster spacecraft in the near-Earth magnetotail on 26 September 2005. The reconnection rate is found to be 3.7–4.8 mV/m; the reconnection distance is around 9–11 Re in the tail.

Citation: Ivanova, V. V., V. S. Semenov, T. Penz, I. B. Ivanov, V. A. Sergeev, M. F. Heyn, C. J. Farrugia, H. K. Biernat, R. Nakamura, and W. Baumjohann (2007), Reconstruction of the reconnection rate from Cluster measurements: Method improvements, *J. Geophys. Res.*, *112*, A10226, doi:10.1029/2006JA012183.

1. Introduction

[2] Observational phenomena referred to as flux transfer events (FTEs) were first observed during crossings of the magnetopause made by the ISEE 1 and 2 spacecraft [*Russell and Elphic*, 1978]. These are transient, ~1-min timescale disturbances characterized by an isolated bipolar variation of the magnetic field component normal to the current sheet and a simultaneous deflection in the tangential components. They were interpreted as disturbances caused by a magnetic flux tube connecting the interplanetary and the Earth's magnetic fields and moving along the magnetopause with a speed greater than the ambient plasma flow [*Russell and Elphic*, 1978]. FTEs are considered to be manifestations of unsteady (impulsive) reconnection at the dayside magnetopause.

[3] The term NFTE was introduced [*Sergeev et al.*, 1992] to emphasize the impulsive nature and profound similarity between magnetopause FTEs and magnetotail reconnection events. NFTE is topologically different from the so-called plasmoid or flux rope. Both objects (plasmoid/flux rope and NFTE structure) are bulges with a typical scale of a few *Re* propagating in the plasma sheet and producing similar perturbations in the tail lobes: the bipolar B_z variation (where z is the direction normal to the current sheet) and the B_x compression over the bulge. However, unlike the plasmoid/flux rope (which have a closed loop magnetic structure) the NFTE bulge carries locally open magnetic flux (see Figure 1). As a consequence, the bipolar B_z signature of NFTEs is typically asymmetric. Though the remotely observed signatures of the objects compared are basically similar, they are interpreted from different points of view: NFTEs are considered to be manifestations of impulsive reconnection on a single X-line, whereas variations associated with plasmoids/flux ropes are interpreted on the basis of MXR reconnection model (multiple X-line reconnection) characterized by the simultaneous existence of two (or more) X-lines.

[4] Analysis of FTEs/NFTEs may provide information about the geometry of the reconnected flux tubes and the reconnection process responsible for their generation. Since spacecraft trajectories sometimes miss a moving flux tube and sample only perturbations outside [*Farrugia et al.*, 1987], the analysis is usually applied to perturbations caused by field line trapping around the flux tube (the bulge), in which case we talk of remote sensing. Modeling this trapping by an isentropic field-aligned MHD flow over gently sloping two-dimensional (2-D) obstacle, *Walthour et al.* [1993, 1994] developed a technique to recover cross-sectional size, shape, orientation, and speed of propagation of FTE structures. Unfortunately, the technique do not suggest any estimation of the most important parameters of reconnection: the rate and the location of the X-line. A method based on the plasmoid interpretation of reconnection events was suggested by *Hu and Sonnerup* [2001, 2003] and *Hasegawa et al.* [2006]. It allows to reconstruct a magnetic map of a plasmoid and is based on a numerical solution of the Grad-Shafranov equation, which describes the evolution of space plasma structures in quasi-static equilibrium. As initial values for the Grad-Shafranov equation, magnetic field and plasma data collected by spacecraft

[1]Institute of Physics, State University, St. Petersburg, Russia.
[2]Space Research Institute, Austrian Academy of Sciences, Graz, Austria.
[3]Institute of Physics, University of Graz, Graz, Austria.
[4]INAF—Osservatorio Astronomico di Palermo, Palermo, Italy.
[5]Petersburg Nuclear Physics Institute, Gatchina, Russia.
[6]Institute for Theoretical Physics, Technical University of Graz, Graz, Austria.
[7]Institute for the Study of Earth, Oceans, and Planets, University of New Hampshire, Durham, New Hampshire, USA.

0148-0227/07/2006JA012183$09.00

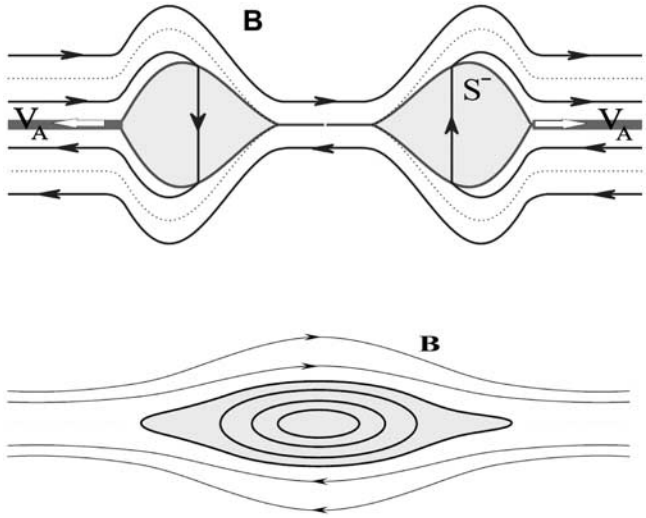

Figure 1. Magnetic structure of the NFTE bulge (according to the model of time-dependent Petschek-type reconnection) and of the plasmoid/flux rope (according to the model of multiple X-line reconnection).

along some trajectory are used. However, an essentially time-dependent process, like reconnection, can hardly be understood in the quasi-static approach. One more technique was introduced by *Fuselier et al.* [2005], providing a snapshot of the reconnection inflow velocity into the magnetosphere and an estimate of the distance from the spacecraft to the reconnection site. These two quantities are not obtained independent of one another, and some additional information is needed to separate them. Being based on a reconnection geometry at the magnetopause rather than on a physical model, the method requires at least two spacecraft staying in a reconnection layer at the same time.

[5] Recently, a new remote sensing method for reconstructing the reconnection rate and the location of X-line from single-spacecraft data was suggested and applied to three NFTEs recorded by Cluster spacecraft in the Earth's magnetotail on 8 September 2002 [*Semenov et al.*, 2005]. From the mathematical point of view, such a reconstruction is an inverse problem: if the reconnection rate $E(t)$ is known, one can compute the temporal profile of the magnetic field $B(t)$ (direct solution); conversely, if $B(t)$ is known, the reconnection rate $E(t)$ can be recovered (inverse solution). To invert the problem an analytical representation of the corresponding direct solution is needed. The analytical model of reconnection developed by Semenov et al. generalizes the classic Petschek mechanism [*Petschek*, 1964] for the nonstationary case and provides a family of direct solutions: 2-D [*Heyn and Semenov*, 1996] and 3-D [*Semenov et al.*, 2004], compressible and incompressible. The model predicts an asymmetric bipolar variation in the magnetic field component normal to the current sheet, a simultaneous deflection in the tangential component, and a change from upward (away from the current sheet) to downward flow in the normal component of plasma velocity, typical for FTE/NFTE disturbances.

[6] The reconstruction method developed by *Semenov et al.* [2005] exploits the most simple variant of the model, namely, 2-D symmetric reconnection in an incompressible plasma. In the present study the method is generalized to include plasma compressibility and possible asymmetry of plasma and magnetic field parameters. Additionally, the accuracy of the reconstruction code has been improved substantially. As a result, numerical noise has disappeared and the range of the code applicability has been expanded.

2. Model

[7] In the frame of the time-dependent Petschek-type model [*Heyn and Semenov*, 1996; *Semenov et al.*, 2004] reconnection is initiated by a local time-varying electric field $E(t)$. A typical initial configuration for reconnection consists of two plasma domains with oppositely directed magnetic fields B_0 and $\tilde{B}_0$ separated by a current sheet. The whole space splits into two different areas: a convective region, where diffusion effects are neglected and the plasma is considered to be ideal, and a vanishingly small diffusion region, where some kind of dissipative process may depress the conductivity thus leading to an electric field $E = j/\sigma$ (j is the current density, σ is the plasma conductivity). As a consequence, the frozen-in property breaks down allowing the magnetic field to reconfigure. The rate at which magnetic field lines reconnect is defined by the dissipative electric field $E(t)$. The question about the precise dissipative mechanism responsible for this field lies outside the model. Since no analytical relation between this mechanism and the electric field is available, the reconnection rate $E(t)$ is taken as an arbitrarily prescribed function. A natural restriction for this function is the causality: $E(t) \equiv 0$ for $t \leq 0$.

[8] To obtain an analytical solution describing further evolution of the magnetic field and plasma configuration several simplifying assumptions are introduced: (1) The plasma domains are uniform. (2) The current sheet, being infinitely thin, is approximated by a tangential discontinuity. (3) The reconnection is "weak," that is, the reconnection electric field $E(t)$ is much smaller than the electric field based on the Alfvén velocity and the background magnetic field $E_A = v_A B_0/c$ [*Petschek*, 1964].

[9] The term "weak" does not mean that the work on plasma is accomplished in a weak manner. On the contrary, regardless of a precise value of the reconnection electric field $E(t)$ plasma is accelerated to the Alfvén velocity. The electric field value influences only the total amount of accelerated plasma. Unlike the first two assumptions (which are rather crude for the case of the magnetosphere) the approximation of weak reconnection is realistic. Different numerical simulations including MHD, Hall MHD, full particle, and hybrid simulations have shown that the reconnection rate is typically of the order of $E \sim 0.1-0.2\ E_A$ [*Birn et al.*, 2001]. The restriction of weak reconnection allows to apply a linear perturbation theory expanding in powers of the small parameter $\varepsilon = E/E_A$.

[10] The time-varying electric field arising in the diffusion region owing to the local decrease of conductivity launches MHD waves in the surrounding medium. Fast mode waves propagate away from the reconnection site and stimulate plasma convection toward the current sheet. Plasma flows entering the current sheet from both sides violate mass conservation for a tangential discontinuity. To make space for a sink of plasma the current sheet broadens

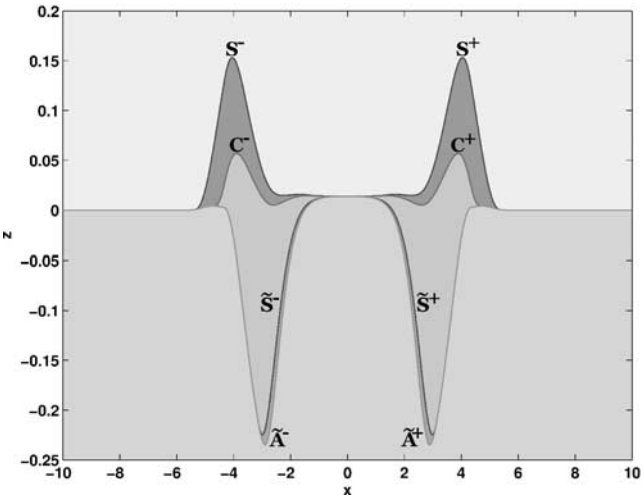

Figure 2. Initial tangential discontinuity, separating two uniform plasma domains with different densities ρ_0, $\tilde{\rho}_0$ and opposite magnetic fields B_0, $\tilde{B}_0$, decays into a system of MHD discontinuities and shocks: S, C, $\tilde{S}$, $\tilde{A}$. A typical structure of *FR* regions is shown at the moment $t = 3$ (switch-off phase). The regions detached from the reconnection site and propagate in opposite directions.

into a system of several MHD discontinuities and shocks [*Heyn et al.*, 1988], which collect the plasma flows and deflect them along the current sheet. In that way two shock structures (left and right) develop filled with accelerated and heated plasma streaming along the current sheet in opposite directions (Figure 2). These structures are referred to as field reversal (FR) or outflow regions. The outer area, where plasma enters from, is named the inflow region.

[11] The curved, water-drop shape of FR regions is due to time variations of the reconnection rate $E(t)$, unlike the original Petschek model, where the rate is constant and FR regions are bounded by straight shocks. Another distinctive feature of time-dependent reconnection is the subdivision of the whole process into two stages: the switch-on phase and the switch-off one. The switch-on phase proceeds, while the electric field in the diffusion region operates leading to the initial decay of the current sheet and the formation of the outflow regions. After the electric field drops to zero and the reconnection switches off, FR regions detach from the reconnection site and propagate away in opposite directions. The volume occupied by the outflow regions grows since it continues to accumulate the ambient plasma.

[12] Within the restriction of "weak" reconnection the FR region is strongly elongated along the current sheet and may be treated as a boundary layer. The number and the type of discontinuities that form the layer depend on the initial configuration (2-D or 3-D, symmetric or asymmetric) and on whether plasma is compressible or not. In a 2-D geometry with moderate asymmetry and compressible plasma the FR structure consists of two slow shocks S, $\tilde{S}$ (which change the magnetic field strength and accelerate plasma), one Alfvén discontinuity A (rotating the magnetic field through the angle π), and a contact discontinuity C (responsible for the density jump) following each other in the order $SC\tilde{S}\tilde{A}$ (Figure 2). It should be mentioned that we neglect the formation of fast shocks because the total pressure across the boundary layer is constant (to the second order of ε), and hence there is no pressure gradient that can drive a fast shock. The Alfvén discontinuity always develops at the side with smaller Alfvén velocity (the lower domain here). Each discontinuity propagates with its own de Hoffmann-Teller velocity and, as a result, the outflow regions are deformed in time.

2.1. Direct Problem

[13] Perturbations of MHD quantities caused by the moving FR structures in the inflow region can be found from the set of compressible ideal MHD equations linearized with respect to the constant background. The final expressions describing the time behavior of magnetic field perturbations at a given point (x, z) in 2-D geometry have a form of integral representations, which relate the perturbations with the reconnection rate $E(t)$ [*Heyn and Semenov*, 1996; *Semenov et al.*, 2004]:

$$B_z(t,x,z) = \frac{B_0}{\pi}\mathrm{Re}\int\limits_{\mathcal{C}} ds \frac{\tilde{L}}{L+\tilde{L}} Q(s)\ is\ E(t-\tau(s)), \qquad (1)$$

$$B_x(t,x,z) = \frac{B_0}{\pi}\mathrm{Re}\int\limits_{\mathcal{C}} ds \frac{\tilde{L}}{L+\tilde{L}} Q(s)q(s)E(t-\tau(s)). \qquad (2)$$

[14] The integrand here is complex, all functions depend on a complex variable s. The integration is carried out in the complex s plane along a special contour defined below.

[15] Throughout the paper, all quantities are normalized with respect to the background magnetic field B_0, the zero-order Alfvén velocity v_a, and the time duration of the electric field pulse. Functions $L(s)$ and $q(s)$ depend on the medium parameters such as the constant background density ρ_0 and zero-order values of the Alfvén speed v_a, the sound speed c_s, and the sum of their squares $u^2 = v_a^2 + c_s^2$:

$$L(s) = -\rho_0 \frac{1+v_a^2 s^2}{q(s)}, \quad q(s) = \sqrt{\frac{1+u^2 s^2 + v_a^2 c_s^2 s^4}{u^2 + v_a^2 c_s^2 s^2}}.$$

$L(s)$ is evaluated for the upper half-space $z > 0$ and $\tilde{L}(s)$ is evaluated for the lower one.

[16] $Q(s)$ is the source (sink) function, which involves all discontinuities and shocks launched by reconnection and thus defines the internal structure of FR regions:

$$\begin{aligned} Q(s) = {} & \left(\frac{1}{B_{SC}} - \frac{1}{B_0}\right)\frac{\mathrm{w}_S^+}{1+is\mathrm{w}_S^+} - \left(\frac{1}{B_{SC}} - \frac{1}{B_0}\right)\frac{\mathrm{w}_S^-}{1+is\mathrm{w}_S^-} \\ & + \left(\frac{1}{B_{\tilde{S}\tilde{A}}} - \frac{1}{B_{C\tilde{S}}}\right)\frac{\tilde{\mathrm{w}}_S^+}{1+is\tilde{\mathrm{w}}_S^+} - \left(\frac{1}{B_{\tilde{S}\tilde{A}}} - \frac{1}{B_{C\tilde{S}}}\right)\frac{\tilde{\mathrm{w}}_S^-}{1+is\tilde{\mathrm{w}}_S^-} \\ & + \left(\frac{1}{\tilde{B}_0} - \frac{1}{B_{\tilde{S}\tilde{A}}}\right)\frac{\tilde{\mathrm{w}}_A^+}{1+is\tilde{\mathrm{w}}_A^+} - \left(\frac{1}{\tilde{B}_0} - \frac{1}{B_{\tilde{S}\tilde{A}}}\right)\frac{\tilde{\mathrm{w}}_A^-}{1+is\tilde{\mathrm{w}}_A^-}. \end{aligned}$$

[17] Here w_S, $\tilde{\mathrm{w}}_S$, $\tilde{\mathrm{w}}_A$ are the de Hoffmann-Teller velocities of the slow shocks and the Alfvén discontinuities, respectively. Plus and minus symbol superscripts refer to

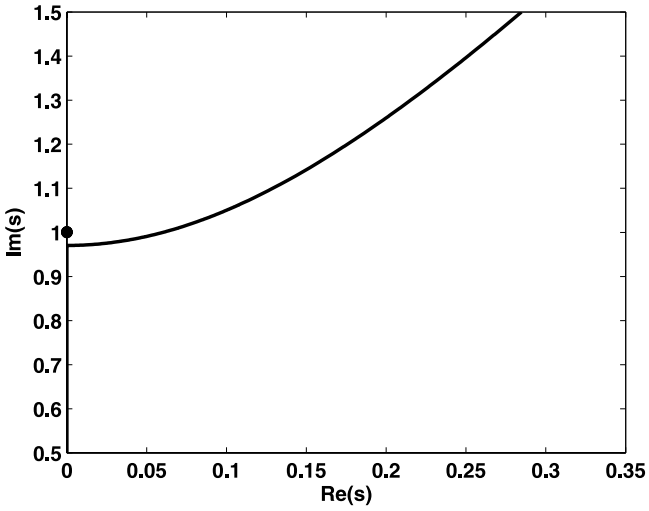

Figure 3. Cagniard contour, calculated for the parameters x = 2, z = 0.5 (dimensionless values). The point indicates the location of the nearest poles.

discontinuities propagating to the right $x > 0$ and to the left $x < 0$ from the diffusion region. The layers between the discontinuities are characterized by a tangential magnetic field marked by a subscript indicating the boundaries. For example, *SC* is the layer between the slow shock and contact discontinuity (Figure 2). The only coordinate-dependent function is

$$\tau(s) = q(s)z - isx, \tag{3}$$

where x and z are counted from the reconnection site located in the origin (0,0).

[18] All poles and branch points originating from the complex integrand lie on the imaginary axis. The branch cuts are chosen in the left half-plane $\mathrm{Re}(s) < 0$. The integration is carried out in the right half of the complex s plane along the so-called Cagniard contour $\mathcal{C}$ (see Figure 3) specified by the requirement that the function $\tau(s)$ is real along it:

$$\mathrm{Im}(\tau(s)) = 0. \tag{4}$$

[19] The integration path stays away from all poles and branch cuts and covers a part of the Cagniard contour between $s = 0$ and the point $s_{\max}$ defined by the causality condition $\tau(s_{\max}) = t$. The Cagniard contour plays a key role in the derivation of the integral representations (1), (2). However, once the formulas (1), (2) are obtained and the endpoint of the integration $s_{\max}$ is defined, the contour can be analytically deformed. For example, it may be deformed to an arc connecting the origin $s = 0$ with $s_{\max}$. To make this, the function $E(t)$ must have an analytical continuation into the complex plane. From the numerical point of view, integration along an arc is more advantageous since there is no need to search for the Cagniard contour (except the point $s_{\max}$).

[20] Typical time variations of magnetic field components predicted by the direct solution (1), (2) for a sample reconnection pulse $E(t) = Ct^2 \exp(-at)$ are shown in Figure 4. To find out the influence of plasma compressibility, the corresponding model variations in an incompressible plasma are presented simultaneously. The comparison between the model curves leads to the following conclusions: (1) B_z and B_x variations show opposite tendencies: the amplitude of the first pulse in the B_z variation increases, whereas in the B_x variation it decreases if the compressibility is taken into account; (2) the perturbation pulse in a compressible plasma is more localized in time; (3) the commencement of the compressible perturbation signal is better pronounced.

[21] The differences/similarities between the model curves may be explained as follows. The form and amplitude of the variations depend on the geometry of the FR region (since the perturbations are caused by field line bending around the FR bulge) and on whether plasma is compressible or not. In a compressible plasma the width of the FR region (in the direction normal to the current sheet) is $\gamma/(\gamma - 1) = 2.5$ ($\gamma = 5/3$) times smaller than in an incompressible one. As a result, the B_x compression over the bulge becomes less efficient (see the smaller amplitude of the compressible B_x variation in Figure 4). Being able to be compressed, a compressible plasma is less sensitive to the bulge movement. It means that magnetic field lines start to bend around the bulge later and hence with greater inclination to the current sheet. This explains the shorter duration of the perturbation signal in a compressible plasma and its more sharp commencement. Owing to a significant curvature of bending field lines the arising B_z component grows more rapidly and reaches greater values at the leading front of the bulge (see the greater amplitude of the first pulse in the compressible B_z variation in Figure 4).

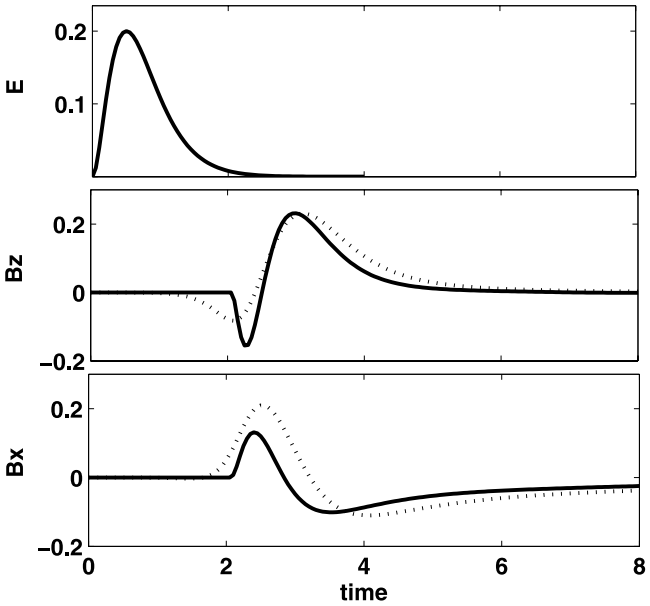

Figure 4. Sample reconnection pulse and the corresponding magnetic field variations at the point x = 2, z = 0.5. Solid lines correspond to a compressible plasma ($\beta = 0.1$) and dotted lines correspond to an incompressible one.

2.2. Inverse Problem

[22] For the inverse problem it is especially important that the direct solution can be written in the form of a convolution. In order to get the convolution representation, the Cagniard contour is again of key importance. Indeed, if the integration in (1), (2) is carried out along the Cagniard contour, it may be done with respect to the real variable τ instead of the complex variable s. The lower integration limit $\tau(s = 0) = z/u$ defines the earliest possible commencement of the perturbation signal (carried by the fast wave propagating with the speed u in the direction perpendicular to the current sheet). Since no disturbance can be detected at the point (x, z) before the moment z/u, there is no contribution to the integral from 0 to z/u and hence the lower limit may be set to zero:

$$B_z(t,x,z) = \int_0^t d\tau K_z(s(\tau))E(t-\tau). \tag{5}$$

[23] Here a short notation K_z for the convolution kernel is introduced:

$$K_z(s) = \frac{B_0}{\pi}\mathrm{Re}\left\{\frac{\tilde{L}}{L+\tilde{L}}Q\frac{is}{\tau'_s}\right\}. \tag{6}$$

[24] The derivative τ'_s has appeared owing to the transformation of the variables $d\tau = \tau'_s ds$. The kernel is presented as a function of the variable s because an explicit expression for $K(\tau)$ is complicated: the fourth-order equation (3), from which the inverse function $s(\tau)$ can be found, has four roots and only one of them should be chosen.

[25] The kernel of convolution characterizes the response of the medium to an elementary, delta-shaped pulse of reconnection. It depends not only on time and the point of observation (x, z) but also involves information about the medium. The compressible asymmetric kernel is much more complicated than the incompressible symmetric one. The analysis of the kernel may resolve all waves and shock structures appearing in the model of Petschek-type reconnection [*Penz et al.*, 2006].

[26] If the temporal profile of the magnetic field perturbation $B_z(t)$ at some observational point (x, z) is known, the relation (5) can be seen as an integral equation for the unknown function $E(t)$. A standard trick to solve an integral equation of convolution type is to perform a Laplace transform with respect to time. In Laplace space, (5) turns to be the simplest algebraic equation, from which the Laplace image of the reconnection electric field can be found as

$$E(p) = \frac{B_z(p)}{K_z(p)}. \tag{7}$$

[27] According to the definition of the direct Laplace transform, the Laplace image of the kernel is

$$K_z(p) = \int_0^\infty K_z(s(\tau))e^{-p\tau}d\tau.$$

On can see that the integration here should be done with respect to the real variable τ, that is, along the Cagniard contour. The possibility to deform the contour does not exist because the function (6) has no analytical continuation into the complex plane.

[28] To find the Cagniard contour (the function $s(\tau)$ for real τ) it is necessary to solve the forth-order algebraic equation (3) and then to choose between four roots an appropriate one (which lies in the first quadrant). Another way is to write equation (3) in a differential form, that is, to demand that the increment of τ along the contour must be strictly real:

$$\mathrm{Im}\left(\frac{d\tau}{dl}\right) = 0, \quad \tau|_{l=0} = z/u,$$

where l is the length parameter along the Cagniard contour. The latter leads to a set of two first-order differential equations (written here as one complex equation):

$$\frac{ds}{dl} = e^{i\phi}, \quad \phi = \arctan\left(\frac{x - \mathrm{Im}(q'_s)z}{\mathrm{Re}(q'_s)z}\right),$$

which define increments of real and imaginary parts of the variable s along the contour. Being supplemented with the initial condition $s(0) = 0$, this set of differential equations gives an alternative way to find the Cagniard contour. From the numerical point of view, this way is more convenient then the choice between the roots because some of the roots are often very close to each other and a wrong root may be chosen. Besides, a numerical solver of differential equations produces an adaptive grid, which is needed for further calculations.

[29] A typical Cagniard contour is shown in Figure 3. First the contour goes along the imaginary axis, then it turns to the right. The turn itself is smooth (though it is not visible in a given scale). The vicinity of the turn is the most important part of the contour and should be calculated with high accuracy since the kernel $K(s)$ has extreme values here. The nearest four poles are located in the vicinity of the point $s = i$. They are not resolved in the scale of Figure 3 and are marked by one point. It should be noted that the Cagniard Contour, being defined by the function $s(\tau)$, depends on the point (x, z), for which the Laplace image of the kernel is calculated.

[30] Now, after the formalism has been discussed, we may return to the main expression (7) and apply it to real spacecraft data, namely, to magnetic variations associated with FTEs. The propagation velocity of FTE structures is several hundred km/s, whereas the spacecraft velocity is only some km/s. Therefore the spacecraft can be considered as fixed in space. A magnetic temporal profile measured by a spacecraft consists of a background magnetic field and a variation. The Laplace image $B_z(p)$ entering the expression (7) has to be calculated for the variation extracted from the magnetic temporal profile.

[31] If the spacecraft coordinates (x, z) (with respect to the reconnection site) are known, the inverse Laplace transform of (7) immediately gives the reconnection rate $E(t)$. In reality, the relative spacecraft location is unknown. To find it, some additional MHD quantity (for example, B_x) is

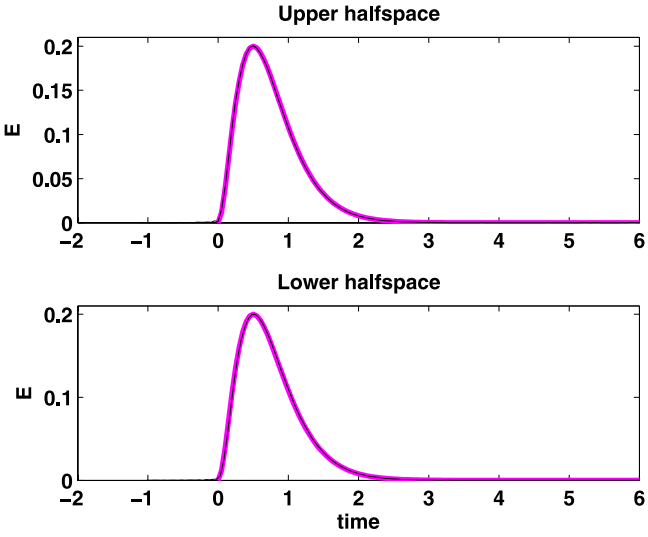

Figure 5. Original (thick magenta line) and the recovered (thin black line) electric pulses, showing (a) the pulse reconstructed from the upper half-space signal at the point $x = 2$, $z = 0.5$ and (b) the pulse reconstructed from the lower half-space signal at the point $x = 2$, $z = -0.5$.

desirable. The algorithm of reconstruction works in the following way. For a given time series $B_z(t)$ and some trial position of the reconnection line one get some reconnection rate $\tilde{E}(t)$. Since the trial coordinates (x, z) are not correct, the rate $\tilde{E}(t)$ usually is negative on a part of the time interval. The real rate must be positive. Therefore the absolute value $|\tilde{E}(t)|$ is taken and the B_z and B_x variations are calculated from it (via the direct solution). Minimizing the standard deviation between the calculated B_z, B_x and those measured by the spacecraft, one can find the optimal reconnection rate $E(t)$ and the position of the reconnection line (x, z) relative to the spacecraft. Minimization is done by a global simulated annealing method.

[32] The reconstruction code has been thoroughly tested for consistency between direct and inverse solutions: it is able to reconstruct $E(t)$ and the distance (x, z) with high accuracy for a wide range of observational points: $0.05 < z/x < 2.5$. Such angular restriction may be explained as follows. The quality of reconstruction depends on the amplitude of the signal: the larger the amplitude, the better the reconstruction results. The amplitude of the signal decreases with z distance and increases with x distance (since the volume of FR region is growing while the region is traveling along the current sheet away from the reconnection site). As a consequence, the reconstruction fails for $z/x > 2.5$. The restriction from below has another origin: in this case the Cagniard contour approaches very close to the poles of the kernel and the accuracy of the calculations falls down.

[33] For real spacecraft data the specified range of applicability should not be perceived literally. We have to remind that the method is based on simplifying assumptions (a homogeneous background with zero normal component of the magnetic field and an infinitely thin current sheet), which are never satisfied with high accuracy.

[34] The improved reconstruction technique may be applied both to symmetric and asymmetric events. A test example of the reconstruction is given for an asymmetric configuration with the background magnetic field $B_0 = 2$ in the upper half-space and $\tilde{B}_0 = -1$ in the lower half-space. The magenta curve in Figure 5 shows the original electric pulse used as an input for the direct problem. The corresponding magnetic field variations calculated for the points $x = 2$, $z = 0.5$ in the upper half-space and $x = 2$, $z = -0.5$ in the lower half-space are presented in Figure 6 by magenta (B_z) and cyan (B_x) curves. The amplitude of variations is smaller in the upper half-space, where the background magnetic field is greater ($B_0 = 2$). The reason is that the enhanced magnetic pressure limits the expansion of the disturbing structure (FR region). The electric pulse reconstructed from the upper half-space signal is shown by the black curve in Figure 5a. The pulse reconstructed from the lower half-space signal is presented in Figure 5b. Naturally, the pulses (corresponding to different input data) are the same. One can see an excellent agreement between the original (thick magenta curve) and the recovered (thin black curve) electric fields. The accuracy of reconstruction crucially decreases for the points lying outside the range of applicability. Some deviation can be already seen, for example, for the point $x = 2$, $z = 5$, which corresponds the upper restriction $z/x = 2.5$. Figure 7 shows the distant (from the current sheet) magnetic field variations in the upper half-space ($x = 2$, $z = 5$) and in the lower one ($x = 2$, $z = -5$). Figure 8 presents the corresponding electric field. The deviation between the original and the recovered curves is visible both in the magnetic perturbations and in the electric pulse.

3. NFTE on 26 September 2005

[35] The generalized method has been applied to NFTE recorded by Cluster spacecraft in the near-Earth magnetotail on 26 September 2005. Application to nightside FTE

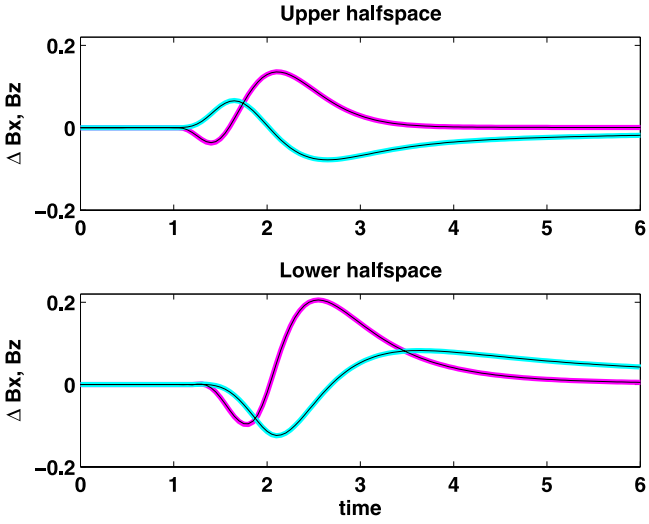

Figure 6. Original and the recovered magnetic field variations at the points (a) $x = 2$, $z = 0.5$ and (b) $x = 2$, $z = -0.5$. The original variations are shown by magenta (B_z) and cyan (B_x) lines and the recovered variations (i.e., corresponding to the recovered electric field) are shown by black line.

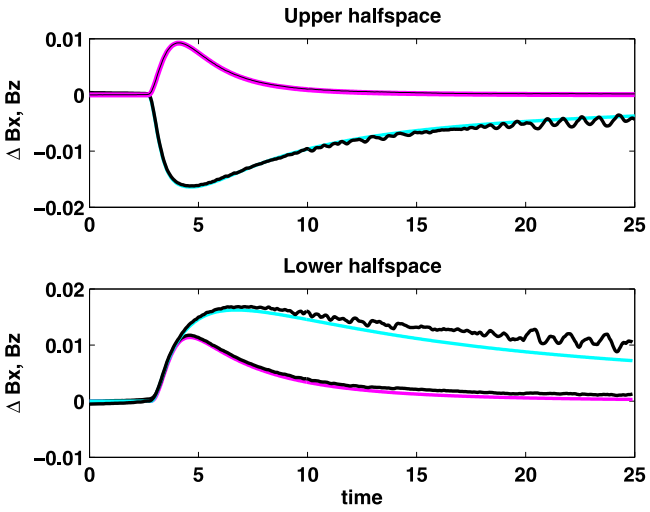

Figure 7. Original and the recovered magnetic field variations at the points (a) $x = 2$, $z = 5$ and (b) $x = 2$, $z = -5$.

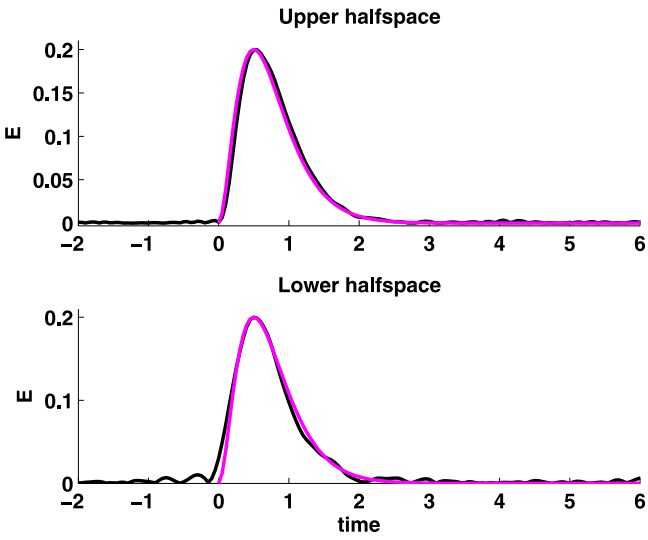

Figure 8. Original (magenta line) and the recovered (black line) electric pulses, showing (a) the pulse reconstructed from the upper half-space signal at the point $x = 2$, $z = 5$ and (b) the pulse reconstructed from the lower half-space signal at the point $x = 2$, $z = -5$.

(which is symmetric) cannot demonstrate the advantage of the extension to an asymmetric configuration. For this purpose a series of dayside FTEs has been examined in a separate paper [*Penz et al.*, 2007]. The present paper demonstrates the difference between compressible and incompressible variants of the reconstruction method.

[36] In contrast to the events analyzed in the previous paper [*Semenov et al.*, 2005], which all took place in the midtail (29–31 Re from the Earth), the event on 26 September 2005 is a rare example of near-Earth reconnection that occurred at a distance $r < 14$ Re. The event was carefully investigated by *Sergeev et al.* [2007]. Observations obtained owing to a fortunate spacecraft configuration (thin current sheet, Hall quadrupole By magnetic field, fast tailward outflow of plasma carrying southward Bz, particle acceleration) reject any doubts that reconnection took place at $r < 14$ Re.

[37] On 26 September 2005, between 0800 and 1000 UT, the Cluster spacecraft moving in a region 14–16 Re in the magnetotail detected three tailward propagating FTE-like disturbances, which were interpreted by *Sergeev et al.* [2007] to be an evidence of near-Earth reconnection. The first event, around 0843, was taken as a test bed for the reconstruction method (Figure 9). At this time all four Cluster spacecraft were located above the current sheet and near the 23 h MLT meridional plane. Since 23 h MLT was the central longitude of the activation [*Sergeev et al.*, 2007], we may consider 3-D effects to be minimal and apply our 2-D reconstruction technique. The later two events are not favorable to apply the method since Cluster spacecraft were crossing the current sheet and distinct magnetic variations can not be obtained.

[38] Around 0843 UT, a strong southward B_z (down to −15 nT), intense GSE E_y (up to 10 mV/m) resulting in tailward outflows with $v_x \sim 400$ km/s, and a strong energetic electron beam (at energy >50 keV) were observed at the spacecraft C2, which was located closest to the neutral sheet [*Sergeev et al.*, 2007]. At the same time other Cluster spacecraft located further away from the neutral sheet did register neither the energetic electron beam nor the fast flows. Apparently, the spacecraft C1, C3 and C4 were staying in the inflow region, whereas C2 crossed the reconnection separatrix and entered the outflow region.

[39] The simplest version of reconstruction presented by *Sergeev et al.* [2007] was based on B_z variation only. The recovered peak rate was ∼4 mV/m, the reconnection pulse duration was ∼100 s, and the location of X-line was around 13–14 Re in the tail. Here we give a more detailed investigation: reconstruction based on both B_z and B_x variations and a comparison with the results of the incompressible variant of the method.

[40] The reconstruction procedure has been applied to three Cluster spacecraft C1, C3, and C4, separately to each of them. The spacecraft C2 has been excluded from con-

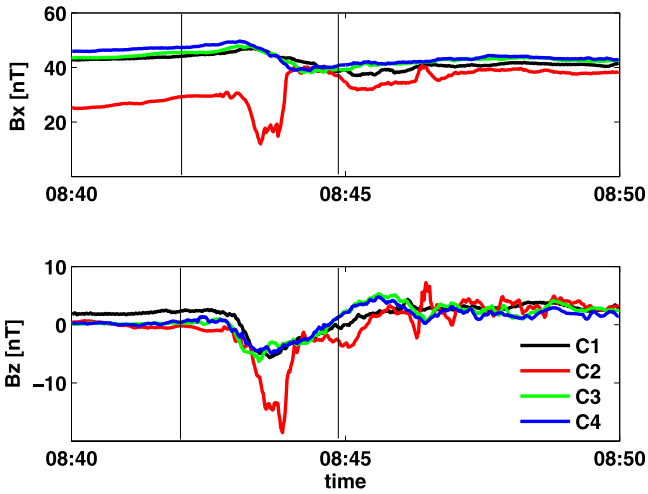

Figure 9. Event on 26 September 2005, observed by four Cluster spacecraft. The interval, chosen for reconstruction, is marked by the vertical lines.

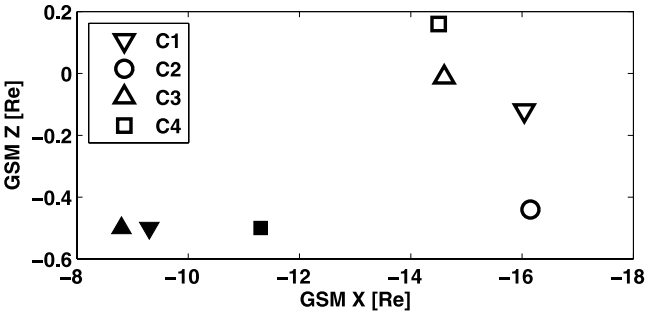

Figure 10. Cluster spacecraft arrangement (empty markers) and the locations of X-line recovered via the compressible procedure (filled markers).

sideration because it was located inside the outflow region and the method is valid only for the inflow region (since it is based on the inverted solution in the inflow region). To prepare the input data, Cluster measurements $B_z(t)$ and $B_x(t)$ have been cut out around 0843 (0842:33–0845:50 for C1 and 0842:00–0844:47 for C3–C4), smoothed, vertically shifted (to subtract the background), and normalized (with respect to the magnetic field value 40 nT and the time interval 60 s). Minimization of the total standard deviation, that is, the sum of standard deviations in B_x and B_z components, was done with respect to both coordinates x and z. A priori information were the spacecraft GSM coordinates and the Alfvén velocity, which is a basic unit for normalization of MHD equations and is needed to convert the results to the dimensional form. The GSM positions of Cluster spacecraft relative to C2 (closest to the neutral sheet) were used to set the lowest possible boundaries for the z distance, which have to be set for the minimization routine: 0.32 Re for C1, 0.43 Re for C3, and 0.60 Re for C4 (see triangle markers in Figures 10 and 11). The Alfvén velocity was estimated from the tailward propagation of the magnetic perturbations: a time delay of about 10 s over ~9000 km separation distance between C3/C4 pair and C1 gives a velocity of ~900 km/s. It should be mentioned, that the accuracy of the reconstruction depends directly on the accuracy of the estimation of the Alfvén velocity. A deviation of the Alfvén velocity from a constant value (owing to violation of the background homogeneity) reduces the accuracy of the method.

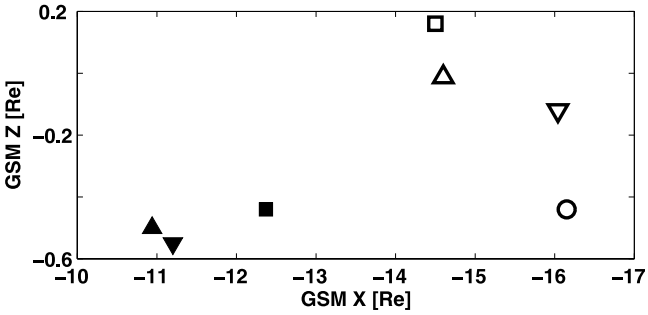

Figure 11. Cluster spacecraft arrangement (empty markers) and the locations of X-line recovered via the incompressible procedure (filled markers).

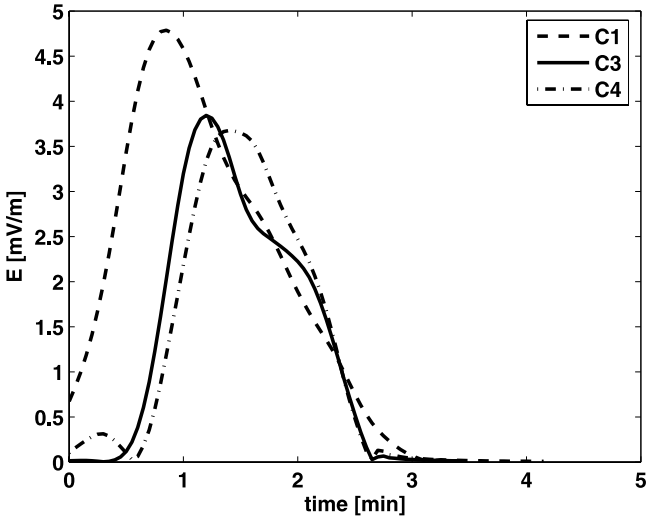

Figure 12. Reconnection electric field reconstructed from Cluster data by the compressible procedure.

[41] Figure 12 shows the reconnection pulse recovered from C1, C3, and C4. The peak rate values vary from 3.7 to 4.8 mV/m and the pulse duration varies from 2 to 3 min. The deviation between the input data and the recovered signal can be seen in Figure 13. Presented are the curves for Cluster C3, but they are typical for all spacecraft. The agreement in B_z is excellent, but the amplitude of B_x is underestimated.

[42] There is also some variability in the X-line location: −9.3 Re for Cluster C1, −8.8. Re for C3, and −11.3 Re for C4 (Figure 10). As already mentioned, the total deviation was minimized with respect to both coordinates x and z. In all cases the minimizing procedure converged to the lowest z boundary (as if the spacecraft C2 was located in the nearest vicinity of the current sheet). Nevertheless, we do not pretend to give an accurate estimate of z distance for this

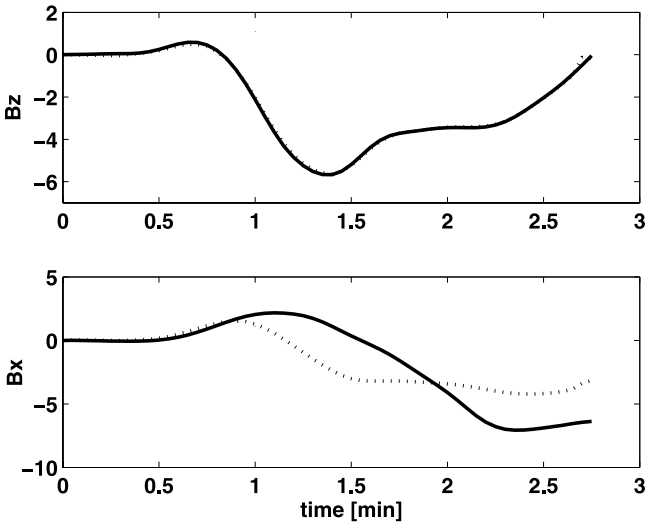

Figure 13. Input signal from spacecraft C3 (solid line) and the signal recovered via the compressible procedure (dotted line).

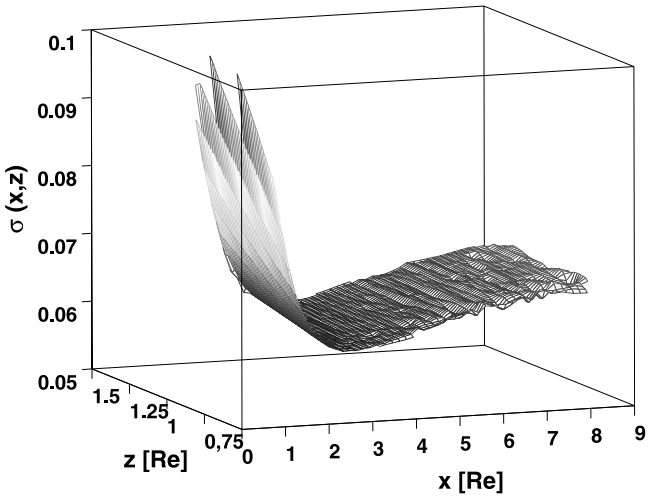

Figure 14. Total standard deviation σ as function of x and z for Cluster C4.

event because the analysis of intermediate minimization results has shown (see Figure 14) that the value of the total standard deviation σ is much more sensitive to the x distance (excluding the range of very small x distances, where the z dependence may be dominant). One can see that the x minimum is well pronounced and, in contrast, the z minimum is not.

[43] To complete the investigation we processed this event by the incompressible routine. The results obtained can be seen in Figure 15 (the reconstructed electric field), Figure 11 (the location of X-line), and Figure 16 (the deviation between the real and the reconstructed data). From the comparison with the compressible results we may conclude the following: (1) The peak values of the reconnection rate are systematically $\sim$1 mV/m smaller in the frame of the incompressible approximation. (2) The duration of the reconnection pulse is nearly the same. (3) The locations of the X-line are systematically shifted farther from the Earth in the incompressible limit: 11–12 Re instead of 9–11 Re. (4) The quality of the reconstruction of the B_x component is nearly the same.

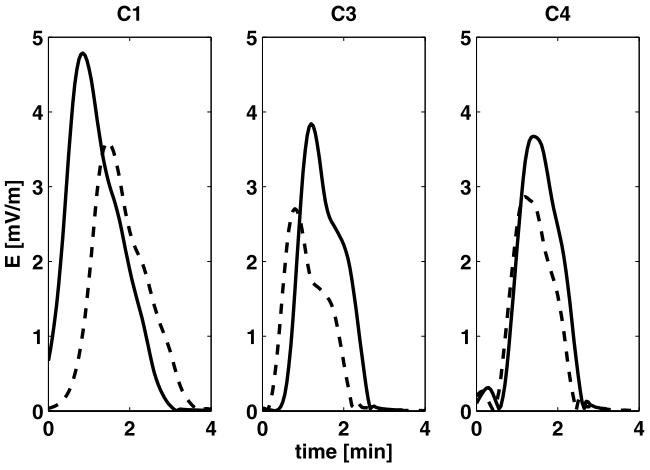

Figure 15. Reconnection electric field reconstructed by the incompressible procedure (dashed lines) in comparison with compressible curves (solid lines).

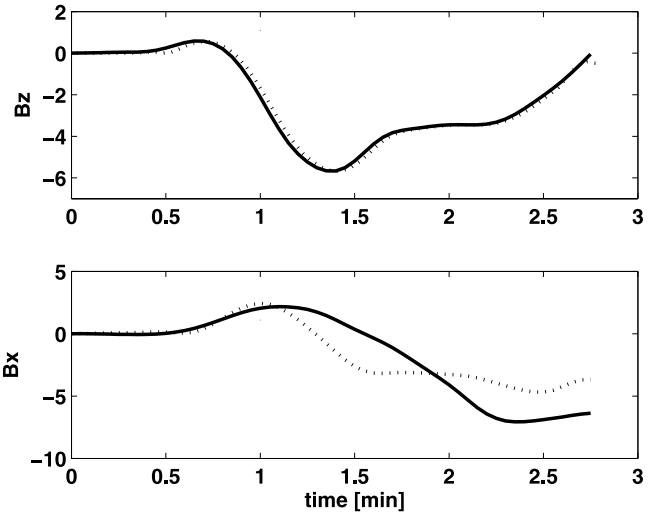

Figure 16. Input signal from spacecraft C3 (solid line) and the signal recovered via the incompressible procedure (dotted line).

[44] The differences between the results reflect some general tendencies typical for the model. To fit the input spacecraft data with more broad incompressible model curves we need a smaller distance between the reconnection site (11–12 Re in the tail) and the point of observation (14–16 Re) (because the volume of FR bulge is growing while the bulge is traveling along the current sheet away from the X-line, and hence the duration of the perturbation signal is getting longer). The smaller electric field value results from the necessity to compensate the greater B_x compression typical for the incompressible limit.

4. Conclusion

[45] In the present paper the reconstruction method developed recently by *Semenov et al.* [2005] has been extended to a compressible plasma and to a configuration with asymmetric plasma and magnetic field parameters. The method allows recovering the reconnection rate and the location of the X-line from single-spacecraft magnetic data.

[46] The improved reconstruction technique has been applied to a nightside flux transfer event recorded by Cluster spacecraft in the near-Earth magnetotail on 26 September 2005. The results obtained (the rate 3.7–4.8 mV/m, the distance 9–11 Re) have been compared with those calculated in the incompressible limit (the rate 2.7–3.8 mV/m, the distance 11–12 Re). The differences between the average peak values of the reconnection rate (3.0 mV/m and 4.1 mV/m) and the average X-line locations (−11.5 Re and −9.8 Re) reconstructed with and without the incompressible approximation are comparable with the variability of the results from different Cluster satellites. The systematic distinction between compressible and incompressible results do exist, but it is not large allowing to conclude that the compressibility is not crucially significant for the event considered.

[47] Being extended to asymmetric configuration, the new technique can be applied to quasi-two-dimensional magnetopause reconnection events. Analysis of two sequences of FTEs seen at the high-latitude magnetopause by the Cluster spacecraft on 14 February 2001 and on 21 January 2001 is already carried out by *Penz et al.* [2007].

[48] **Acknowledgments.** This work is supported by RFBR grant 07–05–00776a, by RFBR/CRDF grant 07–05–91109, by the Austrian "Fonds zur Förderung der wissenschaftlichen Forschung" under project P17099–N08 and by project I.12/04 from the "Österreichischer Austauschdienst." Also acknowledged is support by the Austrian Academy of Sciences, "Verwaltungsstelle für Auslandsbeziehungen." V. V. I. acknowledges support by INTAS "Fellowship Grant for Young Scientists" 04–83–3816. T. P. acknowledges support by the Marie-Curie-Fellowship Contract MTKD–CT–2004–002769 of the project "The influence of stellar high radiation on planetary atmospheres" and the host institution INAF—Osservatorio Astronomico di Palermo. This work is supported in part by NASA grant "Cluster specific theory and modelling" and by NASA grant NNG05GG25G.

[49] Zuyin Pu thanks Hiroshi Hasegawa and another reviewer for their assistance in evaluating this paper.

References

Birn, J., J. F. Drake, M. A. Shay, B. N. Rogers, R. E. Denton, M. Hesse, M. Kuznetsova, Z. W. Ma, A. Bhattacharjee, A. Otto, and P. L. Pritchett (2001), Geospace Environmental Modeling (GEM) magnetic reconnection challenge, *J. Geophys. Res.*, *106*, 3715–3719.

Farrugia, C. J., R. C. Elphic, D. J. Southwood, and S. W. H. Cowley (1987), Field and flow perturbations outside the reconnected field line region in flux transfer events: Theory, *Planet. Space Sci.*, *35*, 227–240.

Fuselier, S. A., K. J. Trattner, S. M. Petrinec, C. J. Owen, and H. Réme (2005), Computing the reconnection rate at the Earth's magnetopause using two spacecraft observations, *J. Geophys. Res.*, *110*, A06212, doi:10.1029/2004JA010805.

Hasegawa, H., B. U. Ö. Sonnerup, C. J. Owen, B. Klecker, G. Paschmann, A. Balogh, and H. Réme (2006), The structure of flux transfer events recovered from Cluster data, *Ann. Geophys.*, *24*, 603–618.

Heyn, M. F., and V. S. Semenov (1996), Rapid reconnection in compressible plasma, *Phys. Plasmas*, *3*, 2725–2741.

Heyn, M. F., H. K. Biernat, R. P. Rijnbeek, and V. S. Semenov (1988), The structure of reconnection layers, *J. Plasma Phys.*, *40*, 235–252.

Hu, Q., and B. U. Ö. Sonnerup (2001), Reconstruction of magnetic flux ropes in the solar wind, *Geophys. Res. Lett.*, *28*, 467–470.

Hu, Q., and B. U. Ö. Sonnerup (2003), Reconstruction of two-dimensional structures in the magnetopause: Method Improvements, *J. Geophys. Res.*, *108*(A1), 1011, doi:10.1029/2002JA009323.

Penz, T., V. S. Semenov, V. V. Ivanova, M. F. Heyn, H. K. Biernat, and I. B. Ivanov (2006), Green's function of compressible Petschek–type magnetic reconnection, *Phys. Plasmas*, *13*, 052108.

Penz, T., C. J. Farrugia, V. V. Ivanova, V. S. Semenov, I. B. Ivanov, S. W. H. Cowley, H. K. Biernat, and R. B. Torbert (2007), Modelled variations of the reconnection electric field at the dayside magnetopause during continued FTE activity, *J. Geophys. Res.*, *112*, A01S90, doi:10.1029/2006JA011937.

Petschek, H. E. (1964), Magnetic field annihilation, in *Physics of Solar Flares*, edited by W. N. Hess, *NASA Spec. Publ.*, *SP 50*, 425–440.

Russell, C. T., and R. C. Elphic (1978), Initial ISEE magnetometer results: magnetopause observations, *Space Sci. Rev.*, *22*, 681–715.

Semenov, V. S., M. F. Heyn, and I. B. Ivanov (2004), Magnetic reconnection with space and time varying reconnection rates in a compressible plasmas, *Phys. Plasmas*, *11*, 62–70.

Semenov, V. S., T. Penz, V. V. Ivanova, V. A. Sergeev, H. K. Biernat, R. Nakamura, M. F. Heyn, I. V. Kubyshkin, and I. B. Ivanov (2005), Reconstruction of the reconnection rate from Cluster measurements: First results, *J. Geophys. Res.*, *110*, A11217, doi:10.1029/2005JA011181.

Sergeev, V. A., R. C. Elphic, F. S. Mozer, A. Saint–Marc, and J. A. Sauvaud (1992), A two-satellite study of nightside flux transfer events in the plasma sheet, *Planet. Space Sci.*, *40*, 1551–1572.

Sergeev, V., et al. (2007), Observation of repeated intense near-Earth reconnection on closed field lines with Cluster, Double Star and other spacecraft, *Geophys. Res. Lett.*, *34*, L02103, doi:10.1029/2006GL028452.

Walthour, D. W., B. U. Ö. Sonnerup, G. Paschmann, H. Lühr, D. Klumpar, and T. Potemra (1993), Remote sensing of two-dimensional magnetopause structures, *J. Geophys. Res.*, *98*, 1489–1504.

Walthour, D. W., B. U. Ö. Sonnerup, R. C. Elphic, and C. T. Russell (1994), Double vision: Remote sensing of a flux transfer event with ISEE 1 and 2, *J. Geophys. Res.*, *99*, 8555–8563.

W. Baumjohann, H. K. Biernat, R. Nakamura, and T. Penz, Space Research Institute, Austrian Academy of Sciences, A-8042 Graz, Austria.

C. J. Farrugia, Institute for the Study of Earth, Oceans, and Planets, University of New Hampshire, Durham, NH 03824, USA.

M. F. Heyn, Institute for Theoretical Physics, Technical University of Graz, A-8010 Graz, Austria.

I. B. Ivanov, Petersburg Nuclear Physics Institute, Gatchina, 188300, Russia.

V. V. Ivanova, V. S. Semenov, and V. A. Sergeev, Institute of Physics, State University, St. Petersburg 198504, Russia. (biglion@inbox.ru)